MATHEMATICAL MODELING AND COMPUTING, Vol. 10, No. 4, pp. 1100–1108 (2023)

Central finite volume schemes for non-local traffic flow models with Arrhenius-type look-ahead rules

Belkadi S., Atounti M.

Mohammed First University,
Multidisciplinary Faculty of Nador, 62702 Selouane-Nador, Morocco

(Received 20 August 2023; Revised 28 October 2023; Accepted 30 October 2023)

We present a central finite volume method and apply it to a new class of nonlocal traffic flow models with an Arrhenius-type look-ahead interaction. These models can be stated as scalar conservation laws with nonlocal fluxes. The suggested scheme is a development of the Nessyah–Tadmor non-oscillatory central scheme. We conduct several numerical experiments in which we carry out the following actions: i) we show the robustness and high resolution of the suggested method; ii) we compare the equations' solutions with local and nonlocal fluxes; iii) we examine how the look-ahead distance affects the numerical solution.

Keywords: *finite volume methods; conservation laws; nonlocal flux; traffic flow modeling; limiters.*

2010 MSC: 35L65, 65M08, 90B20 **DOI:** 10.23939/mmc2023.04.1100

1. Introduction

Many successful macroscopic models have been created and researched to understand the interactions and emergent behaviors of vehicles on the road. These models explain the progress of the density distribution of traffic as opposed to focusing on specific vehicles. The Lighthill–Whitham–Richards (LWR) model is one of the most well-known models of macroscopic traffic flow [1],

$$\partial_t \rho + \partial_x f(\rho) = 0, \quad f(\rho) = \rho v(\rho), \quad v(\rho) = v_{\max}(1-\rho), \tag{1}$$

where $\rho(t,x)$ is the local traffic density, v is a traffic velocity function that only depends on density, and f is the flux.

The flux in (1) is concave and symmetric. However, statistical evidence from traffic networks in the real world indicates that neither a concave nor symmetric flux is expected. Instead, as the density increases, the measured empirical fluxes become right-skewed and convex, as seen in [2].

There are several extensions to the LWR model (1). Consider the nonlocal slowing effect, which states that if there is going to be heavy traffic, drivers will slow down. This requires a nonlocal interaction with a look-ahead distance,

$$\partial_t \rho + \partial_x \left(f(\rho) \exp\left(- \int_0^\eta \kappa_\eta(y) \rho(t, x+y) dy \right) \right) = 0, \quad f(\rho) = v_{\max}\rho(1-\rho), \tag{2}$$

where κ_η is a kernel function. The model was initially published by Sopasakis and Katsoulakis (SK) in 2006 [3] with $\kappa_\eta = 1$, and in 2009, Kurganov and Polizzi proposed a modified version in [4].

Another source of concern is the SK model's fundamental schematic (2). The flux

$$f(\rho) = v_{\max}\rho(1-\rho) \tag{3}$$

is a concave function with even symmetry (concerning $\rho = \frac{1}{2}$), which contradicts experimental results [2]. A non-concave, right-skewed flux appears to be a better fit,

$$f(\rho) = v_{\max}\rho(1-\rho)^\alpha, \quad \alpha > 1. \tag{4}$$

In (4) the flux f is right-skewed and switches from concave to convex at a point $\rho = \frac{2}{\alpha+1}$.

To account for these impacts, we are interested in the following class of traffic models [5]:

$$\partial_t \rho + \partial_x (f(\rho) \exp(-\kappa_\eta * \rho)) = 0, \quad f(\rho) = v_{\max} \rho (1-\rho)^\alpha, \quad \alpha > 1, \tag{5}$$

where

$$\kappa_\eta * \rho(t,x) = \int_x^{x+\eta} \kappa_\eta(y-x)\rho(t,y)\,dy, \quad \eta > 0.$$

The kernel κ_η is a decreasing function such that $\kappa_\eta \in C^1([0,\eta];\mathbb{R}^+)$ and $\int_0^\eta \kappa_\eta(x)\,dx = 1$ (in the numerical section, three different non-negative decreasing kernel functions will be considered: $\kappa_\eta(x) = \frac{1}{\eta}$, $\kappa_\eta(x) = \frac{2}{\eta}\big(1-\frac{x}{\eta}\big)$ and $\kappa_\eta(x) = \frac{3}{2\eta}\big(1-\frac{x^2}{\eta^2}\big)$). Therefore, we define the convolution product as being:

$$U(t,x) = \kappa_\eta * \rho(t,x),$$

and the flux as being:

$$F(\rho,U) = f(\rho)\exp(-U).$$

The formula (5) can be rewritten as follows:

$$\partial_t \rho(t,x) + \partial_x (F(\rho,U)) = 0, \quad x \in \mathbb{R}, \quad t > 0, \tag{6}$$

with the following initial data:

$$\rho(0,x) = \rho_0(x) \in [0,\rho_{\max}]. \tag{7}$$

In this paper, we attempt to study the effect of the nonlocal flux when eta is large (or small enough). We do this by developing an accurate numerical method for the equation (6). Since this model is an extension of (1) with (4), methods designed for scalar conservation laws may be used for the nonlocal flux equation (5). The main methods are finite-volume methods (see, for example, [6–8]), more specifically a class of projection-evolution techniques known as Godunov-type schemes. Godunov's schemes are split into two categories: upwind and central. The approximate solver of the Riemann problem is used in the construction of upwind techniques. Sadly, no Riemann problem solutions exist for the nonlocal flow model (5), therefore upwind approaches can be avoided.

On the other hand, central schemes integrate conservation laws over space-time cells selected in such a way that each Riemann fan is completely contained inside the cell (this is possible due to the finite speed of propagation). As a result, no approximate Riemann problem solution is needed, and central schemes may be expanded to solve our proposed problems. The Lax–Friedrichs (LxF) scheme, [9], is a central scheme prototype. Although it is the much more well-known numerical approach for time-dependent PDEs, despite having a limited resolution. As a result, to improve the LxF scheme's performance, we expand it to a second-order central scheme using the MUSCL (Monotonic Upstream Conservation Laws) approach, which meets the total variation-diminishing (TVD) property.

The following is the manner in which this document is structured: in Section 2, we explain and clarify the second-order central scheme in more detail; in Section 3, we compare the approximate solutions constructed by the proposed central scheme for the problems 6 and 7 with a similar problem but with local flux to show how the calculated solution is dependent on the look-ahead distance. Lastly, in Section 4, we offer some concluding remarks.

2. Central scheme

In this section, we construct the proposed schemes for the new model. We first consider uniform grids and use the following notation: let $x_j = j\Delta x$, $x_{j+\frac{1}{2}} = (j+\frac{1}{2})\Delta x$, $t^n = n\Delta t$, for Δx, $\Delta t > 0$.

Given the cell average of the initial data

$$\rho_j^0 = \frac{1}{\Delta x}\int_{x_{j-\frac{1}{2}}}^{x_{j+\frac{1}{2}}} \rho(0,x)\,dx$$

and the cell average for the exact solution $\rho(t,x)$ of (6) in each cell, $[x_{j-\frac{1}{2}}, x_{j+\frac{1}{2}}]$ at the time level t^n,

$$\rho_j^n \approx \frac{1}{\Delta x}\int_{x_{j-\frac{1}{2}}}^{x_{j+\frac{1}{2}}} \rho(t^n,x)\,dx, \quad j = 1,2,\ldots,N.$$

Second-order accuracy is obtained with the following linear reconstruction from the cell averaged (center) value:

$$\tilde{\rho}^n(x) = \rho_j^n + \delta_j^n(x - x_j), \quad j = 1, \ldots, N, \tag{8}$$

where δ_j^n is a gradient centered on a cell. These gradients are assumed to be constants in each cell, and, therefore, the presence of shocks requires the limitation of the cell-centered gradients in (8).

The choice of adequate limiters is essential in order to obtain accurate and non-oscillatory shock capture. In our numerical tests, we use a generalized minmod limiter (as in [10–12]) with:

$$\delta_j^n = \text{mm}\left(\theta \times \text{mm}\left(\frac{\rho_j^n - \rho_{j-1}^n}{\Delta x}, \frac{\rho_{j+1}^n - \rho_j^n}{\Delta x}\right), \frac{\rho_{j+1}^n - \rho_{j-1}^n}{2\Delta x}\right), \quad \theta \in [1, 2], \tag{9}$$

where the minmod function (denoted as mm) is defined as

$$\text{mm(E)} = \begin{cases} \min(E) & \text{if } E \subset \mathbb{R}^+, \\ \max(E) & \text{if } E \subset \mathbb{R}^-, \\ 0 & \text{otherwise,} \end{cases}$$

and the number θ may be utilized to regulate the numerical viscosity in the final scheme.

We integrate (6) over the space-time cells $[t^n, t^{n+1}[\times[x_i, x_{i+1}[$ and divide two parts by Δx yielding:

$$\frac{1}{\Delta x}\int_{x_j}^{x_{j+1}} \rho(t^{n+1}, x)\, dx = \frac{1}{\Delta x}\int_{x_j}^{x_{j+1}} \rho(t^n, x)\, dx - \frac{1}{\Delta x}\left(\int_{t^n}^{t^{n+1}} F\left(\rho(t, x_{j+1}), U(t, x_{j+1})\right) dt - \int_{t^n}^{t^{n+1}} F\left(\rho(t, x_j), U(t, x_j)\right) dt\right). \tag{10}$$

Defining

$$\rho_{j+\frac{1}{2}}^n = \frac{1}{\Delta x}\int_{x_j}^{x_{j+1}} \rho(t^n, x)\, dx.$$

The staggered averages, $\rho_{j+\frac{1}{2}}^n$ can be computed exactly as

$$\rho_{j+\frac{1}{2}}^n = \frac{1}{\Delta x}\int_{x_j}^{x_{j+1}} \tilde{\rho}(t^n, x)\, dx = \frac{\rho_j^n + \rho_{j+1}^n}{2} + \frac{\Delta x}{8}\left(\delta_j^n - \delta_{j+1}^n\right).$$

The resulting central scheme (10) is then written as follows:

$$\rho_{j+\frac{1}{2}}^{n+1} = \frac{\rho_j^n + \rho_{j+1}^n}{2} + \frac{\Delta x}{8}\left(\delta_j^n - \delta_{j+1}^n\right) - \frac{1}{\Delta x}\left(\int_{t^n}^{t^{n+1}} F\left(\rho(t, x_{j+1}), U(t, x_{j+1})\right) dt - \int_{t^n}^{t^{n+1}} F\left(\rho(t, x_j), U(t, x_j)\right) dt\right). \tag{11}$$

Because of the finite propagation speed, the solution is smooth in the neighborhood next to the points x_j for all j if the following CFL condition is satisfied:

$$\beta < \frac{1}{2\beta_{\max}}, \quad \beta := \frac{\Delta t}{\Delta x},$$

where

$$\beta_{\max} < v_{\max} \max_{\rho \in [0, \rho_{\max}]} \left|\frac{d\left(\rho(1-\rho)^\alpha\right)}{d\rho}\right|.$$

Therefore, the numerical flux is approximated by the second-order mid-point rule:

$$\int_{t^n}^{t^{n+1}} F\left(\rho(t, x_j), U(t, x_j)\right) dt \simeq \Delta t\, F\left(\rho(t^{n+\frac{1}{2}}, x_j), U(t^{n+\frac{1}{2}}, x_j)\right), \tag{12}$$

where the corresponding functions can be evaluated by Taylor's expansion:

$$\rho\left(t^{n+\frac{1}{2}}, x_j\right) = \rho(t^n, x_j) + \tfrac{\Delta t}{2}\rho_t(t^n, x_j), \tag{13}$$

$$U\left(t^{n+\frac{1}{2}}, x_j\right) = U(t^n, x_j) + \tfrac{\Delta t}{2}U_t(t^n, x_j). \tag{14}$$

Compute the terms in (13) and (14). Firstly, from equation (8), we get:

$$\tilde{\rho}_j^n(t^n, x_j) = \rho_j^n.$$

The time derivative ρ_t in (13) is computed with the help of (6),

$$\rho_t(t,x) = -F_x(\rho(t,x), U(t,x)),$$

where the spatial derivative F_x is approximated by the minmod limiters,

$$F_x = \operatorname{mm}\left(\theta \times \operatorname{mm}\left(\frac{F_j^n - F_{j-1}^n}{\Delta x}, \frac{F_{j+1}^n - F_j^n}{\Delta x}\right), \frac{F_{j+1}^n - F_{j-1}^n}{2\Delta x}\right), \tag{15}$$

where

$$F_j = F(\rho_j, U_j) = v_{\max}\rho_j(1-\rho_j)^\alpha \exp(-U_j).$$

We use the midpoint and the composite trapezoidal rule to calculate the terms in (14), and we obtain:

$$\begin{aligned}
U(t^n, x_j) &= \int_{x_j}^{x_j+\eta} \rho(t^n, y)\, \kappa_\eta(y - x_j)\, dy \\
&= \sum_{k=0}^{N-1} \int_{x_{j+k}}^{x_{j+k+1}} \tilde{\rho}^n(y)\, \kappa_\eta(y - x_j)\, dy \\
&= \sum_{k=0}^{N-1} \int_{x_{j+k}}^{x_{j+k+\frac{1}{2}}} \tilde{\rho}^n(y)\, \kappa_\eta(y - x_j)\, dy + \sum_{k=0}^{N-1} \int_{x_{j+k+\frac{1}{2}}}^{x_{j+k+1}} \tilde{\rho}^n(y)\, \kappa_\eta(y - x_j)\, dy \\
&= \sum_{k=0}^{N-1} \left[\kappa_\eta(x_k)\rho_{j+k}^n + \kappa_\eta\big(x_{k+\frac{1}{2}}\big)\left(\rho_{j+k}^n + \delta_{j+k}^n \frac{\Delta x}{2}\right)\right]\frac{\Delta x}{4} \\
&\quad + \sum_{k=0}^{N-1} \left[\kappa_\eta\big(x_{k+\frac{1}{2}}\big)\left(\rho_{j+k+1}^n - \delta_{j+k+1}^n \frac{\Delta x}{2}\right) + \kappa_\eta(x_{k+1})\,\rho_{j+k+1}^n\right]\frac{\Delta x}{4}
\end{aligned}$$

and

$$\begin{aligned}
U_t(t^n, x_j) &= \int_{x_j}^{x_j+\eta} \rho_t(t^n, y)\, \kappa_\eta(y - x_j)\, dy \\
&= -\int_{x_j}^{x_j+\eta} F_y\left(\rho(t^n, y), U(t^n, y)\right) \kappa_\eta(y - x_j) dy \\
&= -\left[\kappa_\eta(y - x_j)\, F\big(\rho\left(t^n, y\right), U(t^n, y)\big)\right]_{x_j}^{x_j+\eta} + \int_{x_j}^{x_j+\eta} \kappa_\eta'(y - x_j)\, F\left(\rho(t^n, y), U(t^n, y)\right) dy \\
&= \kappa_\eta(0)\, F(\rho_j^n, U_j^n) - \kappa_\eta(x_N)\, F(\rho_{j+N}^n, U_{j+N}^n) + \frac{\Delta x}{2}\left[F(\rho_j^n, U_j^n)\,\kappa_\eta'(0) + F(\rho_{j+N}^n, U_{j+N}^n)\,\kappa_\eta'(\eta)\right] \\
&\quad + \Delta x \sum_{k=0}^{N-1} F\big(\rho_{j+k}^n, U_{j+k}^n\big)\,\kappa_\eta'(k\Delta x).
\end{aligned}$$

Finally, the substitution of (12), (13), and (14) in (11) results in our central scheme, which can be written in the following form:

$$\rho_{j+\frac{1}{2}}^{n+1} = \frac{\rho_j^n + \rho_{j+1}^n}{2} + \frac{\Delta x}{8}\left(\delta_j^n - \delta_{j+1}^n\right) - \beta\left(F\big(\rho_{j+1}^{n+\frac{1}{2}}, U_{j+1}^{n+\frac{1}{2}}\big) - F\big(\rho_j^{n+\frac{1}{2}}, U_j^{n+\frac{1}{2}}\big)\right). \tag{16}$$

Remark 1. If $\delta_j = 0$, $\rho\big(t^{n+\frac{1}{2}}, x_j\big) = \rho_j^n$ for all j, thus the second-order central scheme is simplified to the first-order staggered LxF scheme. The resulting first-order scheme is as follows:

$$\rho_{j+\frac{1}{2}}^{n+1} = \frac{\rho_j^n + \rho_{j+1}^n}{2} - \beta\left(F\big(\rho_{j+1}^n, U_{j+1}^n\big) - F\big(\rho_j^n, U_j^n\big)\right), \tag{17}$$

where

$$U_j^n = \Delta x \sum_{k=0}^{N-1} \kappa_\eta(k\Delta x)\rho_{j+k}^n \quad \text{and} \quad F(\rho_j^n, U_j^n) = f(\rho_j^n)\exp(-U_j^n).$$

3. Numerical tests

In this section, we provide a variety of numerical tests to demonstrate how the second-order schemes (16) perform and are particularly appealing for the traffic flow model under consideration. Our objectives are as follows:

— Using a variety of tests, we compare the performance of the proposed central scheme to that of the Lax–F scheme (17).
— Compare the non-local solution to the local solution when the kernel support is large (or small enough).
— Investigating how the computed solution varies with the look-ahead distance

In all our numerical tests, we impose the condition $\eta = N\Delta x$; the CFL number is 0.5; $v_{\max} = 1$; we use periodic boundary conditions for simplicity; and we use a generalized slope limiter with $\theta = 2$. We indicate the form of boundary conditions that are applied for each numerical test. Assuming a uniform partition of $[a, b]$, $\{C_j\}_j^m$ with $\Delta x = \frac{(b-a)}{m}$, we define ρ_j^n in the ghost cells for $j = 1, \ldots, m$ as follows:

$$\rho_0^n = \rho_m^n, \quad \text{and} \quad \rho_{j+m}^n = \rho_j^n \quad \text{for} \quad j = 1, \ldots, N.$$

Since we can not explicitly compute the exact solution, we refined the grid to get a reference solution. Regarding the Lax–Friedrichs schemes, if $\rho_{\Delta x}(T, x)$ and $\rho_{\frac{\Delta x}{2}}(T, x)$ are the solutions calculated with m and $2m$ grid cells, respectively, the L^1 error for the cell average $\rho_{\Delta x}$ is given by

$$\begin{aligned} e(\Delta x) &= \left\| \rho_{\Delta x}(T, \cdot) - \rho_{\frac{\Delta x}{2}}(T, \cdot) \right\|_{L^1} \\ &= \sum_{j=1}^{m} \int_{I_{2j}} \left| \rho_{\Delta x}(T, x) - \rho_{\frac{\Delta x}{2}}(T, x) \right| dx + \int_{I_{2j-1}} \left| \rho_{\Delta x}(T, x) - \rho_{\frac{\Delta x}{2}}(T, x) \right| dx \\ &= \frac{\Delta x}{2} \sum_{j=1}^{m} \left(|\rho_j - \rho_{2j}| + |\rho_j - \rho_{2j-1}| \right), \end{aligned}$$

where

$$C_j = I_{2j-1} \cup I_{2j} \quad \text{and} \quad \rho_{\frac{\Delta x}{2}}(T, x) = \begin{cases} \rho_{2j-1}, & x \in I_{2j-1}, \\ \rho_{2j}, & x \in I_{2j}. \end{cases}$$

The integrals in the second-order central schemes are calculated using a high-order quadrature method; therefore, the L^1 error is determined as

$$\begin{aligned} e(\Delta x) &= \left\| \rho_{\Delta x}(T, \cdot) - \rho_{\frac{\Delta x}{2}}(T, \cdot) \right\|_{L^1} \\ &= \Delta x \sum_{j=1}^{M} \left| \rho_j - \frac{9}{16}(\rho_{2j} + \rho_{2j-1}) + \frac{1}{16}(\rho_{2j+1} + \rho_{2j-2}) \right| \frac{\Delta x}{2}. \end{aligned}$$

In both situations, the convergence order is specified by

$$\gamma(\Delta x) = \frac{\ln(e(\Delta x)) - \ln\left(e\left(\frac{\Delta x}{2}\right)\right)}{\ln(2)}.$$

3.1. Test 1. Comparison of the schemes

We consider the equation (6) with the following initial data:

$$\rho_0(x) = \begin{cases} 1 & \text{if} \quad 0 \leqslant x \leqslant 10, \\ 0 & \text{otherwise.} \end{cases} \tag{18}$$

This is appropriate when the traffic light is at $x = 10$ and changes from red to green at the start of the time interval. We compute the numerical solution of (2)–(18) at time $T = 5$ using $\kappa_\eta = \frac{1}{\eta}$, $\kappa_\eta(x) = \frac{2}{\eta}(1 - \frac{x}{\eta})$ and $\kappa_\eta(x) = \frac{3}{2\eta}(1 - \frac{x^2}{\eta^2})$. We fix $\Delta x = \frac{1}{10}$ and compare the numerical results produced with the second-order central scheme to those obtained with the first-order Lax–Friedrich's scheme. The results are displayed in Figures 1a, 1b, and 1c are compared to the reference solution, which was obtained with the second-order central scheme.

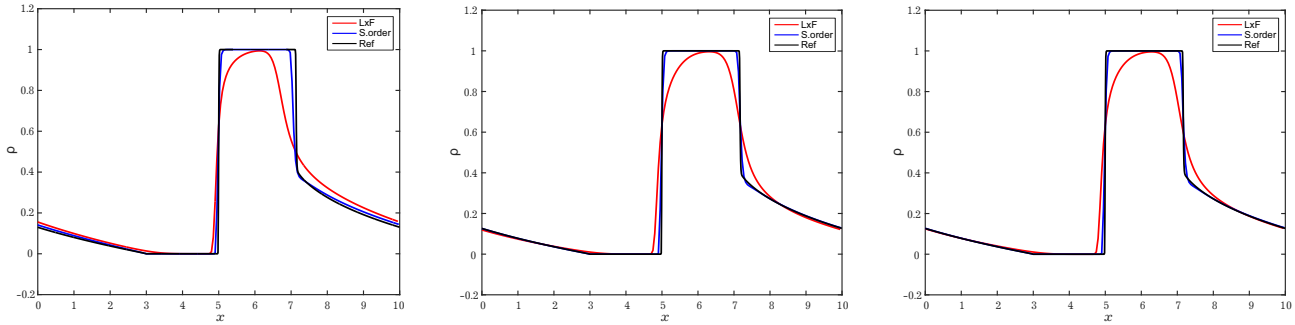

a $(\kappa_\eta(x) = \frac{1}{\eta})$ ***b*** $(\kappa_\eta(x) = \frac{2}{\eta}(1 - \frac{x}{\eta}))$ ***c*** $(\kappa_\eta(x) = \frac{3}{2\eta}(1 - \frac{x^2}{\eta^2}))$

Fig. 1. Comparison of numerical solutions computed with the second-order central scheme and Lax–Friedrich's scheme using $\Delta x = \frac{1}{10}$ and $\eta = 0.1$ at $T = 5$, corresponding to the initial condition (18) and different kernel functions. The reference solution is computed using a second-order central scheme with $\Delta x = \frac{1}{100}$.

Figure 1 shows the results for different kernel functions. The numerical results obtained by the second-order central scheme are appropriate approximations of shocks and rarefaction waves. The second-order central schemes are better than Lax–Friedrichs schemes at capturing the reference solution for the shock waves, while the former's solutions are more diffusive.

3.2. Test 2. Convergence order

To determine the correct rating of the schemes (16) and (17) in terms of accuracy, we now examine the initial data given below:

$$\rho_0(x) = \begin{cases} 0.8 & \text{if} \quad -1/3 \leqslant x \leqslant 1/3, \\ 0.2 & \text{otherwise}, \end{cases} \tag{19}$$

for $x \in [-1, 1]$ and compute the approximate solutions at $T = 1$ for various kernel functions with $\eta = 0.1$. The results are given in Table 1.

Table 1. L^1 error and convergence orders using various kernel functions and $\eta = 0.1$ for the initial condition (19).

Scheme		$\kappa_\eta = \frac{1}{\eta}$		$\kappa_\eta = \frac{2}{\eta}(1 - \frac{x}{\eta})$		$\kappa_\eta = \frac{3}{2\eta}(1 - \frac{x^2}{\eta^2})$	
	$\frac{1}{\Delta x}$	L^1 error	$\gamma(\Delta x)$	L^1 error	$\gamma(\Delta x)$	L^1 error	$\gamma(\Delta x)$
S.order	40	5.8914e-04	—	5.6440e-04	—	5.6564e-04	—
	80	1.7837e-04	1.72	1.4507e-04	1.96	1.4358e-05	1.97
	160	4.2055e-05	2.08	3.4213e-05	2.08	3.5470e-05	2.01
	320	1.1782e-05	1.83	9.0058e-06	1.92	9.2867e-06	1.93
	640	2.9148e-06	2.01	2.3252e-06	1.95	2.4753e-06	1.90
Lax–F	40	5.6300e-02	—	5.9000e-02	—	5.8200e-02	
	80	3.7600e-02	0.58	3.9900e-02	0.56	3.9400e-02	0.56
	160	2.3300e-02	0.69	2.4600e-02	0.69	2.4400e-02	0.69
	320	1.5900e-02	0.55	1.6900e-02	0.54	1.6700e-02	0.54
	640	9.8000e-03	0.69	1.0500e-02	0.68	1.0300e-02	0.69

Table 1 shows the L^1 errors and numerical accuracy orders $\gamma(\Delta x)$ for both schemes. We computed numerical approximations with $\frac{1}{\Delta x} = 10 \times 2^k$ for $k = 2, 3, \ldots, 6$. The L^1 error of the second-order schemes is smaller than the Lax–Friedrichs errors for each step of refinement, which is a clear indication that the error of the second-order central schemes diminishes as the mesh is refined. In conclusion, we may compare the performance of the second-order schemes with that of the first-order scheme when the solution has discontinuities.

3.3. Test 3. Numerical comparisons between local and nonlocal solutions when η is large or small enough

As in Test 3.1, we apply the proposed central schemes to (6), (18) and a similar problem with local flux, and we compute its solutions on a uniform grid with $\Delta x = 0.1$ for various η values at the time

final $T = 20.20$. The solutions are shown in Figures 2 and 3. It is easy to see the impact of the nonlocal flux that reflects the look-ahead rules. The effect is especially clear in the wave's head, where the density wave corresponding to the nonlocal situation visibly follows behind the local one. This can be explained by being vigilant when cars are coming. At the same time, because the interaction potentials for cars at the front of the wave vanish, the nonlocal and local solutions are nearly identical. Finally, we show how the computed solution is affected by the look-ahead distance, η. Figure 4 shows the solutions produced using the second-order central scheme for $\eta = 0.1, 0.2, 0.4, 0.8$ and $\eta = 1, 2, 4, 8$ are shown in Figure 5. As can be observed, there is a high reliance on η: as η diminishes, drivers can see less, which reduces their sensitivity to contact and causes the initial traffic congestion to dissipate more quickly. The nonlocal flow, however, is not very significant when η is quite large.

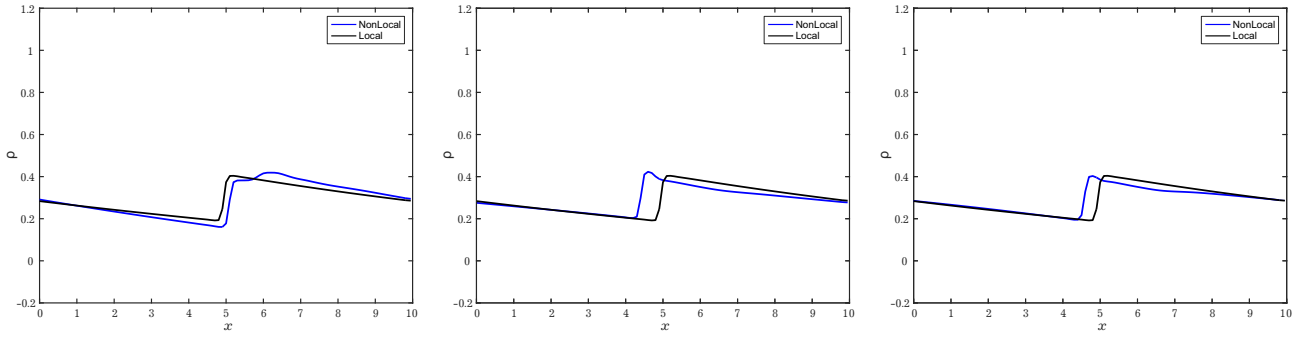

a $(\kappa_\eta = \frac{1}{\eta})$ ***b*** $(\kappa_\eta(x) = \frac{2}{\eta}(1 - \frac{x}{\eta}))$ ***c*** $(\kappa_\eta(x) = \frac{3}{2\eta}(1 - \frac{x^2}{\eta^2}))$

Fig. 2. The effect of look-ahead dynamics: nonlocal vs. local fluxes. The solution to (6) computed with a different kernel function and $\eta = 8$, $T = 20$.

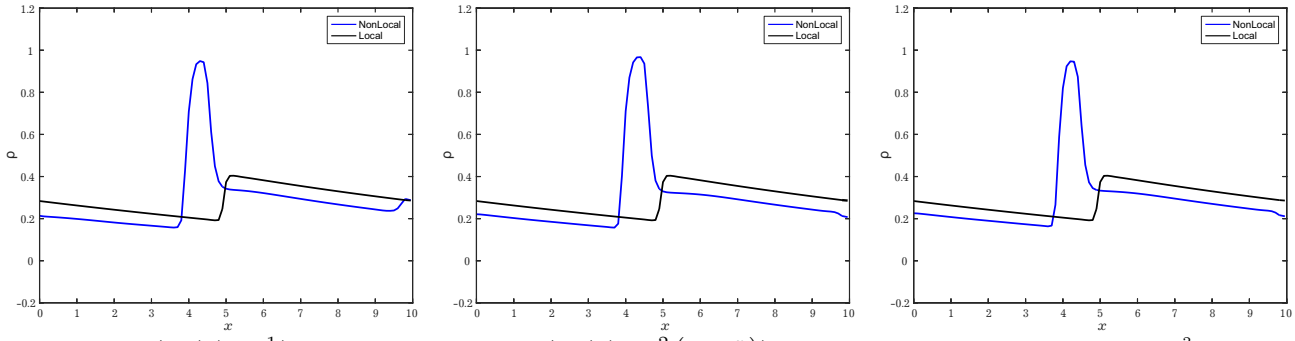

a $(\kappa_\eta(x) = \frac{1}{\eta})$ ***b*** $(\kappa_\eta(x) = \frac{2}{\eta}(1 - \frac{x}{\eta}))$ ***c*** $(\kappa_\eta(x) = \frac{3}{2\eta}(1 - \frac{x^2}{\eta^2}))$

Fig. 3. The effect of look-ahead rules: nonlocal vs. local fluxes. The solution to (6) computed with a different kernel function and $\eta = 0.1$, $T = 20$.

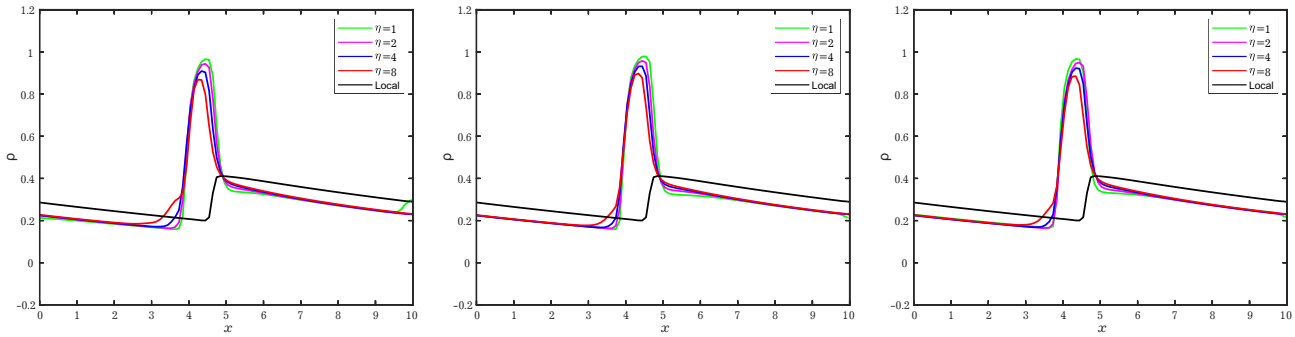

a $(\kappa_\eta(x) = \frac{1}{\eta})$ ***b*** $(\kappa_\eta(x) = \frac{2}{\eta}(1 - \frac{x}{\eta}))$ ***c*** $(\kappa_\eta(x) = \frac{3}{2\eta}(1 - \frac{x^2}{\eta^2}))$

Fig. 4. The solution to (6) computed with different kernel functions and decreasing values of $\eta = 0.8$, 0.4, 0.2, 0.1; $T = 20.20$.

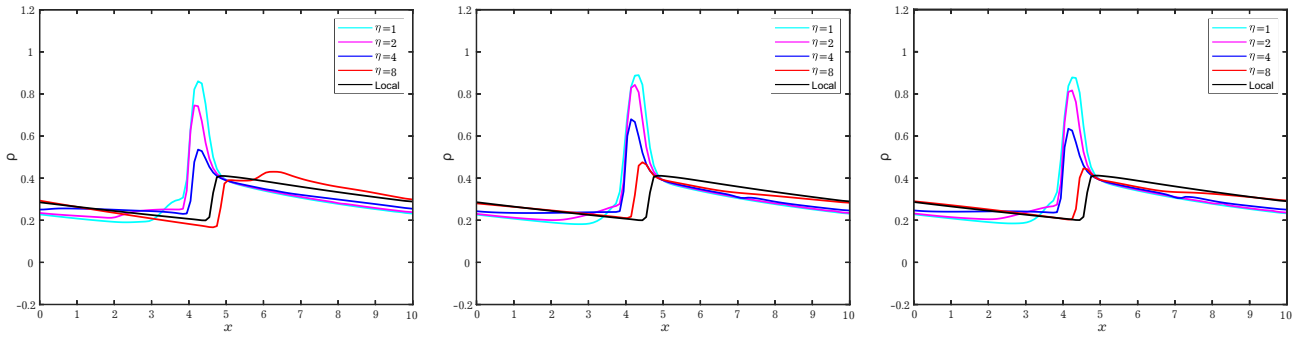

a $(\kappa_\eta(x) = \frac{1}{\eta})$ ***b*** $(\kappa_\eta(x) = \frac{2}{\eta}(1 - \frac{x}{\eta}))$ ***c*** $(\kappa_\eta(x) = \frac{3}{2\eta}(1 - \frac{x^2}{\eta^2}))$

Fig. 5. The solution to (6) computed with a different kernel function and increasing values of $\eta = 1, 2, 4, 8$, $T = 20.20$.

To further elucidate the dependence of the computed solution on the look-ahead distance η, we compute the L^1 distance between the approximate solutions obtained for the central second-order scheme applied to (6)–(18) and the solution of a traditional (LxF) scheme for the equivalent local equation. The corresponding L^1 distances shown in Table 2 decrease when η is large enough. Figure 5 illustrates the results in more detail.

Table 2. L^1 distances between the approximate solutions ρ_L and ρ_η to the local model and the nonlocal model, respectively, for different η at $T = 20.20$ with different kernel functions for the initial condition (18).

	$\|\rho_\eta - \rho_L\|_{L^1}$		
η	$\kappa_\eta = \frac{1}{\eta}$	$\kappa_\eta(x) = \frac{2}{\eta}\left(1 - \frac{x}{\eta}\right)$	$\kappa_\eta(x) = \frac{3}{2\eta}\left(1 - \frac{x^2}{\eta^2}\right)$
1	0.8326	0.8977	0.8776
2	0.6602	0.7628	0.7341
4	0.4028	0.5594	0.5168
8	0.2477	0.2229	0.1628

4. Conclusion

We extended and studied the central accurate numerical method for nonlocal traffic flow models with look-ahead rules. Our numerical method extends the second-order reconstruction-based schemes for local conservation laws in the sense that, as the nonlocal variable disappears, we regain the well-known second-order central scheme for the local equation. We created the second-order approach that converges to the unique solution if the convolution kernel and the look-ahead distance meet certain conditions. We performed many numerical experiments that compared our proposed scheme to the first-order method proposed in [13, 14]. The nonlocal solution provided by the second-order central scheme is also more accurate than the solution obtained by the Lax–Friedrichs scheme. Hence, the reliance on η is substantial: as η diminishes, drivers can see more, lowering their attention to contact and causing the original traffic congestion to clear more slowly. When η is quite large, however, the influence of the nonlocal flux is negligible. Our numerical results also showed that the choice of the flux function influences the development of shocks in the nonlocal model.

[1] Lighthill M., Whitham G. B. On kinematic waves. II. A theory of traffic flow on long crowded roads. Proceedings of the Royal Society A. **229** (1178), 317–345 (1995).

[2] Kuhne R. D., Gartner N. H. 75 Years of the Fundamental Diagram for Traffic Flow Theory: Greenshields Symposium. Transportation Research Board E-Circular (2011).

[3] Sopasakis A., Katsoulakis M. A. Stochastic modeling and simulation of traffic flow: asymmetric single exclusion process with Arrhenius look-ahead dynamics. SIAM Journal on Applied Mathematics. **66** (3), 921–944 (2006).

[4] Kurganov A., Polizzi A. Non-oscillatory central schemes for a traffic flow model with Arrhenius look-ahead dynamics. Networks and Heterogeneous Media. **4** (3), 431–451 (2009).

[5] Lee Y. Thresholds for shock formation in traffic flow models with nonlocal-concave-convex flux. Journal of Differential Equations. **266** (1), 580–599 (2019).

[6] Eymard R., Gallouët T., Herbin R. Finite Volume Method. Handbook of Numerical Analysis. Lions, Janvier (2013).

[7] Godlewski E., Raviart P. A. Hyperbolic Systems of Conservation Laws. Ellipses (1991).

[8] Helbing D., Treiber M. Gas-kinetic-based traffic model explaining observed hysteretic phase transition. Physical Review Letters. **81** (14), 3042–3045 (1998).

[9] Chiarello F. A., Goatin P. Global entropy weak solutions for general non-local traffic flow models with the anisotropic kernel. ESAIM: M2AN. **52** (1), 163–180 (2018).

[10] Belkadi S., Atounti M. Non-oscillatory central schemes for general non-local traffic flow models. International Journal of Applied Mathematics. **35** (4), 515–528 (2022).

[11] Nessyahu N., Tadmor E. Non-oscillatory central differencing for hyperbolic conservation laws. Journal of Computational Physics. **87** (2), 408–463 (1990).

[12] Sweby P. K. High-resolution schemes using flux limiters for hyperbolic conservation laws. SIAM Journal on Numerical Analysis. **21** (5), 995–1011 (1984).

[13] Blandin S., Goatin P. Well-posedness of a conservation law with non-local flux arising in traffic flow modeling. Numerische Mathematik. **132** (2), 217–241 (2017).

[14] Goatin P., Scialanga S. Well-posedness and finite volume approximations of the LWR traffic flow model with non-local velocity. Networks and Heterogeneous Media. **11** (1), 107–121 (2016).

Центральні схеми скінченного об'єму для нелокальних моделей транспортних потоків із правилами прогнозу типу Арреніуса

Белкаді С., Атунті М.

Перший університет Мухаммеда,
Багатопрофільний факультет Надора, 62702 Селуан–Надор, Марокко

Представлено центральний метод скінченного об'єму та його застосування до нового класу моделей нелокального трафіку з прогнозованою взаємодією типу Арреніуса. Ці моделі можна сформулювати як скалярні закони збереження з нелокальними потоками. Запропонована схема є розвитком неосциляційної центральної схеми Нессія–Тадмора. Проведено декілька чисельних експериментів, у яких виконано такі дії: i) продемонстровано надійність і високу роздільну здатність запропонованого методу; ii) порівняно розв'язки рівнянь з локальними та нелокальними потоками; iii) перевірено, як відстань уперед впливає на чисельний розв'язок.

Ключові слова: *методи скінченного об'єму; закони збереження; нелокальний потік; моделювання транспортного потоку; обмежувачі.*